

Dielectric Relaxation of a Polybutadiene Melt at a Crystalline Graphite Surface: Atomistic Molecular Dynamics Simulations

Mathieu Solar, Kurt Binder and Wolfgang Paul

Abstract Dielectric experiments are an indispensable tool to further our understanding of the relaxation behavior of polymers, not only in bulk samples but also in confined situations. A chemically realistic Molecular Dynamics simulation, in which all information about molecular motions is available, can shed light onto the questions of heterogeneity and anisotropy of the underlying molecular relaxation processes which lead to the ensemble averaged experimental dielectric signal. In this contribution, we present a careful analysis of the dielectric response of a weakly polar and confined polymer, 1,4-polybutadiene between graphite walls. The relaxation of the segmental dipole moments was obtained in the time domain and transformed into frequency (Fourier) domain as well as the relaxation time (Debye) domain to highlight the differences between the two types of analysis. A particular bonus of the simulation is that detailed spatially resolved information on structure and dynamics of the confined system is available. We determine the influence of the confinement on the dielectric relaxation and show that for this system the apparent glass transition temperature of a confined film is independent of its thickness even on the scale of a few nanometers.

Keywords Interphase · Molecular Dynamics · Confinement · Coarse-grained model · Atomistic simulations · Dynamic heterogeneity · Polybutadiene · Graphite walls · Dielectric relaxation · Fluctuation-dissipation theorem · Fourier transform · Laplace transform · Dielectric loss spectrum · Relaxation time distribution ·

M. Solar (✉) · W. Paul

Institut für Physik, Martin-Luther-Universität Halle-Wittenberg, 06099 Halle (Saale), Germany
e-mail: mathieu.solar@physik.uni-halle.de

W. Paul

e-mail: wolfgang.paul@physik.uni-halle.de

K. Binder

Institut für Physik, Johannes-Gutenberg-Universität, 55099 Mainz, Germany
e-mail: kurt.binder@uni-mainz.de

Alpha-process · Vogel/Fulcher/Tammann equation · Relaxation map · Glass transition temperature · Torsion stiffness · Layering · Anisotropic relaxation

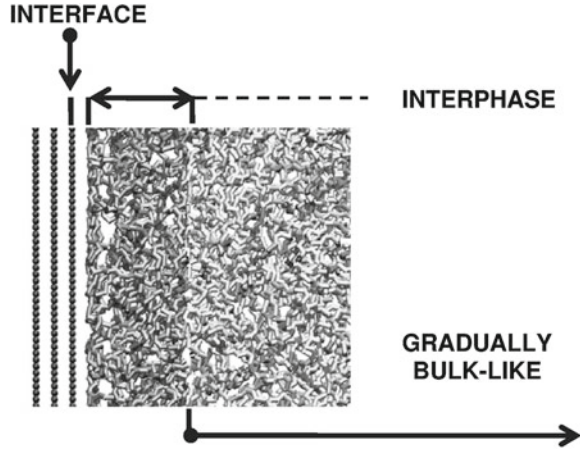
Abbreviations

DIP	Dipole moment
DSC	Differential Scanning Calorimetry
FFT	Fast Fourier Transform
KWW	Kohlrausch-Williams-Watts
MD	Molecular Dynamics
NMR	Nuclear Magnetic Resonance
PBD	PolyButaDiene
RTD	Relaxation Time Distribution
vdW	van der Waals
VFT	Vogel/Fulcher/Tammann

1 Introduction

Dielectric spectroscopy is an important technique to address the dynamics of macromolecular systems [1]. It measures the polarization current of a (loaded) sample capacitor. Thus, the relaxation of the projection of the electric dipole moment of the sample onto the applied electric field can be measured. For polymeric systems, local dipole moments are carried by some or all of the segments making up the chains, so the total dipole moment is a sum of the segmental ones, $\mu_{\text{tot}} = \sum_i \mu_i$. The macroscopic dipole density in a volume V is then given as $\mathbf{p} = (1/V) \cdot \sum_i \mu_i$. In linear response theory, the dielectric permittivity tensor $\epsilon = \epsilon_{\alpha\beta}$ links the polarization to the external electric field \mathbf{E} by the relation $\mathbf{p} = (\epsilon - \mathbf{1})\epsilon_0\mathbf{E} = \chi\epsilon_0\mathbf{E}$, where χ is the dielectric susceptibility tensor and ϵ_0 is the dielectric permittivity of vacuum. The dielectric signal in the time domain is then proportional to $\langle [\mathbf{p}(t) \cdot \mathbf{E}(t)][\mathbf{p}(0) \cdot \mathbf{E}(0)] \rangle \propto \langle \mu_{\text{tot},E}(t)\mu_{\text{tot},E}(0) \rangle$, where the angular brackets indicate a thermodynamic average and the index, E , denotes the projection onto the applied electric field. In most polymers, the individual segmental dipoles relax essentially independently, so one has $\langle \mu_{\text{tot},E}(t)\mu_{\text{tot},E}(0) \rangle \propto \langle \mu_{\text{seg},E}(t)\mu_{\text{seg},E}(0) \rangle$, and the experiment probes local segmental relaxation. In so-called type A polymers, the dipole components perpendicular to the chain backbone relax independently, but the parallel components are correlated and add up to a dipole moment parallel to the chain end-to-end vector. In these polymers, dielectric spectroscopy can address local (segmental) as well as global (end-to-end vector) conformational relaxation of polymer chains, and separates into the so-called “segmental” and “normal” modes. Molecular Dynamics (MD) simulations addressing the dielectric response of a polymer melt have been mostly concerned with bulk systems, see [2–4] for example. These

Fig. 1 Snapshot of a polymer melt close to a crystalline surface. The interphase is the region perturbed by the confinement where any physical property gradually evolves to a bulk-like behavior far away from the surface



systems are homogeneous and isotropic and the susceptibility is proportional to the unit tensor, $\chi = \chi \delta_{\alpha\beta}$. Then the dielectric observable is proportional to the auto-correlation function of the dipole vector, $\langle \mu_{\text{tot},E}(t) \mu_{\text{tot},E}(0) \rangle \propto \langle \mu_{\text{tot}}(t) \cdot \mu_{\text{tot}}(0) \rangle$. It has been found in experiments [5] as well as in simulations [3] that the assumption of uncorrelated relaxation of different segments discussed above seems to be a good approximation to describe bulk dielectric behavior.

The development of polymer nanocomposite materials required to go beyond the analysis of bulk dielectric behavior and led to the study of confined polymer systems, where the confinement may be one-dimensional (films) or two-dimensional (nanopores). One then has to address the question what changes occur in the polymer dynamics at a solid surface and what may be the characteristic width of the perturbed region in the polymer, the so-called “interphase” (see Fig. 1). Clearly, the relaxation behavior in such a confined system becomes heterogeneous, i.e., it depends on the distance to the surface, as well as anisotropic: an electric field applied perpendicular to the surface probes other molecular motions than a field applied parallel to the surface. For a flat (i.e., atomically corrugated) surface, the susceptibility tensor is written as $\chi = \chi_{\alpha} \mathbf{e}_{\alpha} \otimes \mathbf{e}_{\alpha}$ in a Cartesian basis \mathbf{e}_{α} ; $\alpha = x, y, z$. Due to the rotational symmetry, one has $\chi_x = \chi_y \neq \chi_z$ and correspondingly for the dielectric permittivity. The dielectric relaxation of a polymer film was first analyzed carefully for a computer simulation in a study of Peter et al. [6], who considered, however, a coarse-grained bead-spring polymer model supported by a perfectly smooth and flat repulsive interface. This study was motivated by the question, how the glass transition behavior of a polymer melt is changed in a polymer film, a controversial topic in the study of the glass transition phenomenon, which had received much experimental, e.g., [7–9], and simulation attention, e.g., [10–14]. This question is closely related to the problem whether or not the dramatic slowing down of relaxation phenomena in glass forming fluids is associated with the growth of a lengthscale over which motions are strongly correlated [15]. This idea is well established for continuous

phase transitions in equilibrium systems (“critical slowing down”), but the extent to which this mechanism can be carried over to glassy freezing is heavily debated [15].

In the following, we discuss the dielectric relaxation of a melt of 1,4-polybutadiene (PBD) chains confined by two parallel graphite surfaces, simulated in a chemically realistic way. We present in detail also the technical aspects of determining the dielectric relaxation behavior for such a chemically realistic simulation. The next section discusses our model and the simulation technique. In Sect. 3, we then present the determination of the dielectric response from the MD simulation trajectory, both in the time domain and in the frequency domain. This section addresses the questions of anisotropy and heterogeneity of the dipolar relaxation. In Sect. 4, we then address the analysis of the temperature dependence of the segmental relaxation and its dependence on film thickness. In addition, the determination of the relaxation time distribution (RTD) from the simulations is discussed in Sect. 5 and finally Sect. 6 presents some conclusions.

2 Atomistic MD Simulations of PBD Between Graphite Walls

We performed MD simulations in the NVT ensemble (i.e., at constant density and temperature) extending for up to approximately 1 μ s in time using the Gromacs package [16]. The simulations were performed for a chemically realistic model of 1,4-polybutadiene (55 % trans, 45 % cis) for which the dielectric relaxation functions in the bulk have been studied before [3]. The polymer melt consisted of N_c chains each of $N_p = 116$ united atom particles representing CH, CH₂ and CH₃ (treated as CH₂) groups, i.e., the chains consisted of 29 repeat units. The force field for the polymer melt may be found in the literature [17]. The graphite model was taken from the literature as well [18] and standard Lorentz-Berthelot combining rules were applied. The glass transition for this polymer¹ was estimated at $T_g = 178$ K from differential scanning calorimetry (DSC) measurements, and at $T_g = 175$ K from rheological measurements [19]. The PBD melt was confined between two graphite walls, which were 10 nm ($T = 353$ K, 323 K, 293 K, 273 K, 253 K and then $N_c = 720$) and 20 nm ($T = 240$ K, 225 K and 213 K and then $N_c = 1440$) apart, respectively. Periodic boundary conditions were applied in the three Cartesian directions to simulate a semi-infinite polymer film confined between two half-spaces of graphite. The temperature of the melt was kept fixed using a Nosé-Hoover thermostat, whereas the carbon atoms were frozen. The Newton equations were integrated using a leap-frog algorithm with a timestep of $\delta t = 1$ fs. Since we are considering a weakly polar polymer at a neutral interface, the influence of the partial atomic charges on the segmental dynamics can be neglected (same as for the bulk [20]), so that the atomic charges

¹ In Ref. [19], a polymer with 7 % of 1, 2, 52 % of 1,4-trans and 41 % of 1,4-cis fractions was considered.

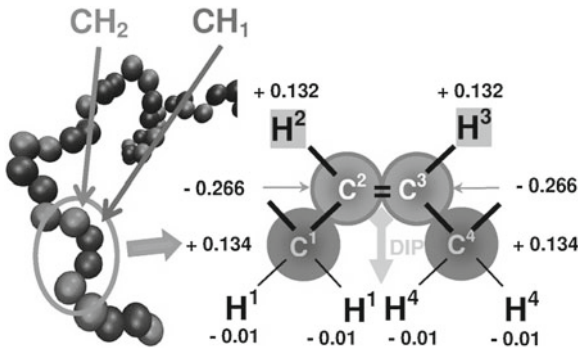


Fig. 2 The *left* picture shows a snapshot of one polymer chain consisting of a repetition of the monomeric unit $\text{CH}_2\text{--CH}=\text{CH--CH}_2$. A cis conformation is isolated and shown with the real charges on the *right* [3]. The dipole moment (DIP) of the cis segment is computed using the position of the particles. The hydrogen atoms lie on bisections between carbon triplets

were not included in the MD simulations to speed-up the calculations. Thus, the dielectric properties were estimated *a-posteriori* by reinserting partial charges into the stored trajectories as shown in Fig. 2. For the bulk, this procedure gave results which were in quantitatively good agreement with dielectric experiments [3], NMR spin lattice relaxation time measurements [21] and neutron spin echo measurements of the chain dynamics [22]. Each chain in the PBD melt contains 13 cis and 16 trans conformations in a random sequence. A trans conformation has no dipole moment, so that only the segmental relaxation of the cis-conformations is observed in the dielectric spectroscopy experiment.

3 The Dielectric Relaxation of PBD at Graphite

To illustrate the effect that the presence of the graphite wall has on the structure of the melt adjacent to it, we show in Fig. 3 the dependence of the particle density and the chain center of mass density profiles as a function of the distance from the next wall. The crystalline graphite surface attracts the united atoms through a van der Waals attraction. This attraction leads to a strong density layering. Similarly, an adsorbed layer is observable in the center of mass density. With decreasing temperature the layering in the particle density becomes sharper, but the distance over which this layering extends, does not grow significantly in the simulated temperature range. These structural changes influence the relaxation behavior of the polymer segments and lead to a heterogeneous response, depending on the distance to the walls, but only on the scale of a few nanometers, as one would expect from Fig. 3.

Due to the presence of the attraction to the walls, motions parallel (x , y) and perpendicular (z) to the walls are also not equivalent, so one has heterogeneous as

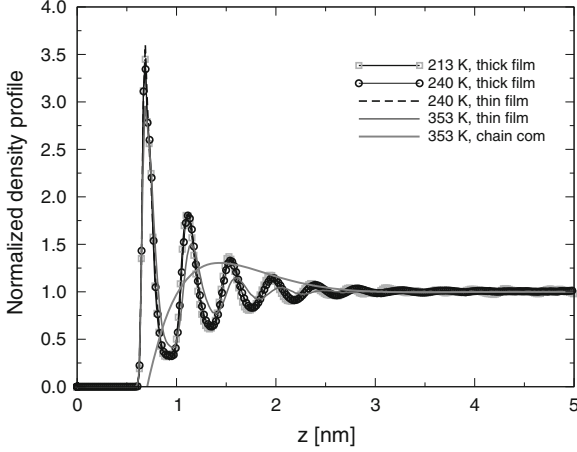


Fig. 3 Particle and chain center of mass density profiles. All densities are normalized to their values in the center of the film, where the particle density is equal to the bulk density at this temperature

well as anisotropic dynamics. In a dielectric experiment on a thin polymer film, the support will always provide one of the electrodes, so that the electric field is oriented perpendicular to the walls. According to the discussion in the introduction, the dielectric experiment is then sensitive to the relaxation of the z -component of the total dipole moment or respectively the segmental dipole. The measured dielectric permittivity is then $\varepsilon = \varepsilon_{zz}$. The most interesting behavior of the segmental relaxation function is observed for a layer of segments directly adjacent to the walls, which is shown in Fig. 4. The dipole relaxation functions in Fig. 4 are not describable as a simple exponential decays $\phi(t) = \exp(-t/\tau_0)$, where t is time and τ_0 the relaxation time constant. After a short time vibrational decay, which is visible in the log-lin plot in the inset and which happens on times below 1 ps, there are two more processes observable.

They can be clearly seen at the higher temperatures but seem to merge at the lower temperatures. The first of these is the structural relaxation (or α -relaxation) of the system, the second one an additional decay process linked to the wall-desorption kinetics [23, 24]. It is known, that the α -process is well described by a stretched exponential decay (Kohlrausch-Williams-Watts, KWW, law) $\phi(t) = \exp[-(t/\tau_{\text{KWW}})^\beta]$, where the stretching exponent obeys $0 < \beta < 1$ and τ_{KWW} is the time constant. We empirically fitted the relaxation functions in Fig. 4 by a sum of two stretched exponentials to capture the two relaxation processes present,

$$\phi(t) = a_0 \left[a_1 \exp \left[-(t/\tau_0)^{\beta_0} \right] + (1 - a_1) \exp \left[-(t/\tau_1)^{\beta_1} \right] \right], \quad (1)$$

where a_0 , a_1 , τ_0 , β_0 , τ_1 and β_1 are the fitting parameters. The overall amplitude, a_0 , is smaller than one because the short time vibrational decay can not be captured by

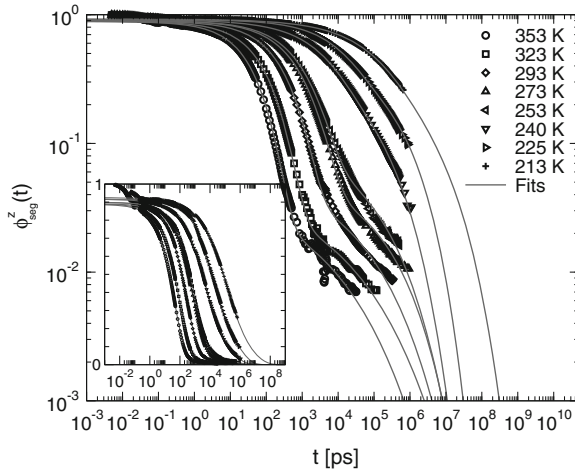


Fig. 4 Main panel: log—log representation of the segmental dipole relaxation functions as a function of temperature. The relaxation functions were computed for a layer of width 1.2 nm next to the walls. The functional form of Eq. (1) was fitted to the data (*grey full lines*). Small panel: log—lin representation of the same data

this fit. For the center region of the film, the final wall-induced relaxation process is absent (data not shown) and a single exponential is enough to fit the autocorrelation functions, in the same way as for the bulk.

3.1 The Dielectric Loss Spectra

The relaxation functions in Fig. 4 span many decades in time and contain processes on very different time scales, from the fast vibrational motions to the long time desorption kinetics. To obtain these functions requires a logarithmic sampling in time, and it is impossible to resolve the whole curve with a resolution adapted to the fastest process. Thus, the raw simulation data were first interpolated and linearly sampled over the full time range of observation, and then a Fast Fourier Transform algorithm was used to obtain the frequency spectrum. In addition, the good fit functions (as shown by the red lines in Fig. 4) at hand were also used to generate the correlation functions on a uniformly spaced time grid of width Δt having 2^{26} time points, which could be used to extend the time range over which the relaxation function was observed compared to the raw data. This was done for all temperatures.

The Shannon-Nyquist sampling theorem then relates the time increment to the largest frequency one can resolve, and the lowest frequency is given by the inverse of the longest time, $(2^{26} \Delta t)^{-1}$, one reaches this way. The time interval Δt depends on temperature because the longest time scale one has to reach increases with decreasing temperature, so the frequency grid points for which one determines the Fourier

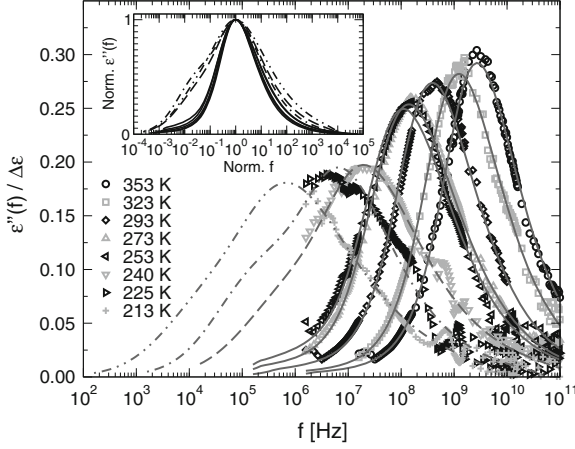


Fig. 5 Main panel: temperature dependence of the dielectric loss for the layer next to the wall. At high temperatures the Fourier transforms of the data and the fit agree, at the lowest temperatures, the Fourier transform of the fit allows for an extrapolation to lower frequencies than obtainable from the data. Inset: scaled representation of the same data showing a broadening of the frequency spectra at low temperatures

transform also depend on temperature. The dielectric spectra shown in Fig. 5 show that the results obtained by transforming the original data and by transforming the fit functions agree with each other for high temperatures. At the lowest temperatures, the relaxation becomes so slow that it can not be completely resolved within the simulation time window. Here the Fourier transforms of the fits (which agree with those of the data at high frequencies) allow for an extrapolation of the spectra to lower frequencies.

4 The Temperature Dependence of the α -Process

The temperature dependence of the position of the maximum in the dielectric loss, which was used in the inset of Fig. 5 to scale the frequencies, gives a measure for the temperature dependence of the α process. When we perform this analysis for different layer widths starting at the graphite surface, we can obtain an idea on the thickness dependence of the glass process in PBD films. This temperature dependence is not described by an Arrhenius law in fragile glass formers to which PBD belongs, rather it is empirically fitted by the Vogel/Fulcher/Tammann (VFT) equation [15]

$$f = f_{\infty} \exp \left[- \frac{E_a}{(T - T_0)} \right], \quad (2)$$

or

Table 1 Results of VFT fits (see Fig. 6) adjusted to the data from the MD simulations

Param.	Bulk	1.2 nm	2.5 nm	3.7 nm	5.0 nm
$\log(f_\infty)$	11.405 ± 0.061	10.758 ± 0.152	10.884 ± 0.128	10.986 ± 0.131	11.027 ± 0.131
E_a	980 ± 53	664 ± 43	691 ± 37	721 ± 39	739 ± 40
T_0	141 ± 5	155 ± 1	153 ± 1	151 ± 1	149 ± 1
T_g	173 ± 7	178 ± 3	176 ± 2	175 ± 3	174 ± 3

The glass transition temperature and its (asymptotic standard) error bar are estimated from the fit parameters using Eq. (3)

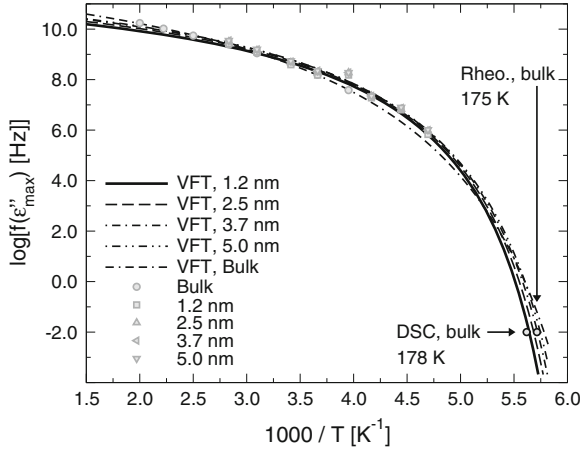


Fig. 6 The relaxation map for various layer thicknesses. The error in the data is smaller than the size of the symbols. The respective thicknesses are given in the legend. The *lines* show empirical VFT fits (see Table 1), extrapolating to the known bulk glass transition temperature within the error bars

$$T = T_0 + \frac{E_a}{[\ln f_\infty - \ln f]}, \quad (3)$$

where f_∞ (frequency as $T \rightarrow +\infty$), E_a (activation temperature) and T_0 (so-called ideal glass transition or Vogel temperature) are the fitting parameters. We recall that one model that leads to Eqs. (2) or (3) is based on the idea of regions where relaxations require cooperative rearrangements of the molecules (or monomeric units) that they contain, implying that the size of these regions diverges at T_0 . However, the empirical fits of actual data show (see Table. 1) that T_0 always is distinctly smaller than T_g .

The second form allows for the calculation of the glass transition temperature when the VFT parameters are known. The glass transition temperature corresponds to a relaxation rate of $f = 10^{-2}\text{Hz}$ [25]. Therefore, one may define here the dielectric glass transition by $T_g = T(f = 10^{-2}\text{Hz})$ [1]. When one performs VFT fits to the data in Fig. 6, one obtains the fit parameters shown in Table 1, where also the error bars of the fit parameters are given.

There is an obvious jump in the value of the Vogel temperature T_0 going from the bulk to the film data. The reason for this is the change in the temperature range for which the data are available. The bulk data are taken from Ref. [3] and are given for $253\text{K} \leq T \leq 500\text{K}$, whereas the film data are given for $213\text{K} \leq T \leq 353\text{K}$. This jump reveals the fact that the VFT law actually is not able to cover the complete temperature dependence from the high temperature liquid to the supercooled regime close to T_g . This was worked out in pioneering dielectric experiments by Stickel et al. [26, 27] and was also found for simulations on bulk PBD [20], when the time scale for incoherent neutron scattering was analyzed. Rather than a VFT law, one has to use two Arrhenius laws to capture the crossover from high temperature liquid-like to low temperature solid-like relaxation. However, when we look at the prediction for the glass transition temperature obtainable from these VFT fits, we can conclude that they agree with each other and with the experimentally known value within the error bars inherent in the VFT fitting procedure. There is no indication that the glass transition temperature changes with a reduction in film thickness, similar to what is found in recent dielectric experiments, for example in [28, 29]. This conclusion differs from the one reached in the simulation work by Peter et al. [6]. We explain this difference by the difference between a coarse-grained and a chemically realistic model. In a bead-spring coarse-grained model, the glass transition is mostly determined by density effects alone, so a layering as visible in Fig. 3 leads to strong effects on the glass transition temperature. In a chemically realistic model, the internal rotation barriers of the dihedral angles are much more important and induce a larger dynamic chain stiffness than a bead-spring coarse-grained model possesses, where no torsion stiffness is included. Removing the torsion potential from the simulation shifts the glass transition temperature of PBD (simulated at the realistic densities) from about 175 K to about 60 K [2]. The layering at the walls (or for that purpose, the reduced density at a free surface) therefore has a much smaller effect on T_g in such realistic models and in real confined polymer systems then it has for simulations of a coarse-grained model.

5 The Relaxation Time Distribution

It is astonishing that the two processes clearly visible in the time domain behavior (Fig. 4) do not lead to separate peaks in the frequency spectra (Fig. 5). This smearing out of features in the Fourier analysis can be avoided when one instead determines the relaxation spectrum $\rho(\tau)$ (or distribution of relaxation times) of the time domain signal. Here, the relaxation function is written as an integral over Debye processes, i.e.,

$$\phi(t) = \int_0^{+\infty} \rho(\tau) \exp[-t/\tau] d\tau, \quad (4)$$

where one has to fulfill the normalization condition $\int_0^{+\infty} \rho(\tau) d\tau = 1$. Eq. (4) may be reinterpreted as a Laplace transform if one replaces the real variable t by the complex variable $s = \zeta + i\eta$ (i stands for imaginary unit) and carries out a change of variables $\lambda = 1/\tau$. It leads to Eq. (5), where the function $\bar{\rho}(\lambda) = \rho(1/\lambda)/\lambda^2$ should be reinterpreted as a spectrum of relaxation rate constants, which is simpler to use from a mathematical point of view. From there, the function $\bar{\rho}$ of λ can be calculated as the inverse Laplace transform \mathcal{L}_ϕ^{-1} of the relaxation function ϕ using the variable s . It follows that

$$\mathcal{L}_{\bar{\rho}}(s) = \int_0^{+\infty} \bar{\rho}(\lambda) \exp[-s\lambda] d\lambda, \quad (5)$$

$$\bar{\rho}(\lambda) = \frac{1}{2\pi i} \int_{\zeta - i\infty}^{\zeta + i\infty} \phi(s) \exp[+s\lambda] ds. \quad (6)$$

Since the function ϕ , see Eq. (1), as a function of $s = \zeta + i\eta$ belongs to the Hardy space (i.e., ϕ is a holomorphic function for $\Re(s) > 0$ and $\sup_{\zeta > 0} \int_{-\infty}^{+\infty} |\phi(\zeta + i\eta)|^2 d\eta < +\infty$), the Paley-Wiener theorem allows one to set ζ to zero in equation (6), i.e., the inverse Fourier transform of $\phi(i\eta)$ exists, and $\bar{\rho}$ is a square-integrable function (i.e., $\int_{-\infty}^{+\infty} |\bar{\rho}(\lambda)|^2 d\lambda < +\infty$), see [30, 31]. Thus, the inverse Laplace transform may be written as an inverse Fourier transform. The relaxation rate distributions were computed for each model $\phi(t)$ using the FFT algorithm, after the function ϕ was normalized. The computation was done for several integration time windows, so as to cover a large range of relaxation rate constants. We carefully checked that the normalization condition was satisfied, and that the relaxation rate distributions obtained give the model $\phi(t)$ according to Eq. (4). Finally, one can convert the results into distributions of relaxation time constants.

The RTD is able to separate the two processes as shown in Fig. 4 and to reveal their temperature dependence. This dependence is shown in Fig. 7 the layer of width 1.2 nm next to the wall for which the contribution of the desorption process is clearest. For both processes, the typical relaxation times increase as the temperature is lowered, however, the time scale for the α -relaxation increases faster than the one for the desorption process. Thus the two peaks first merge and the relative position of the two contributions even changes. In addition and for a given temperature, in Fig. 7, a big red filled circle corresponds to the frequency of the maximum dielectric loss from Fig. 5. Doing this for the temperature range that was simulated, one obtains a master line, which indicates that the maximum dielectric loss position in frequency is a blend of the two processes. One can also conclude that different physics of the glass transition may be addressed, if one considers the maximum dielectric loss or the maxima in the relaxation rate distributions.

It is interesting to perform a direct comparison of the analysis in terms of a superposition of Debye processes and the analysis in terms of a superposition of harmonic oscillators (Fourier spectrum). We perform this comparison in Fig. 8 for

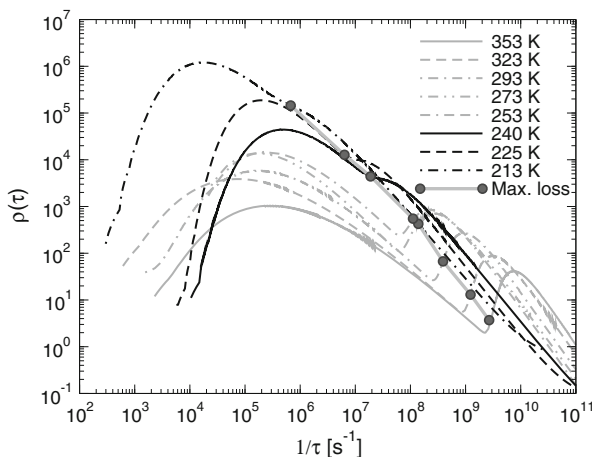


Fig. 7 The temperature dependence of the relaxation time distributions as a function of the relaxation rate constant (equivalent to the inverse of the relaxation time constant) for the layer next to the wall. The big *filled circles* are located at the frequency of maximum dielectric loss from Fig. 5

the relaxation behavior observed in layers of different thicknesses next to the walls and for a temperature of 353 K. Clearly, the Fourier signal shows a single peak which only broadens upon reducing the layer thickness for which the dielectric signal is evaluated (only for the smallest thickness of 1.2 nm there is a small shift of the peak position). Both relaxation processes contribute to this peak and the stronger contribution of the wall process for the smaller layer thicknesses only leads to the observed broadening. In contrast, for the RTD a clear bimodal signal is observed. The peak at lower τ captures the contributions to the α process at this temperature, the peak at larger τ captures the wall-desorption process. The latter one is completely absent when one considers a layer in the center of the film as shown by the dashed line.

6 Conclusion

In this contribution, MD simulations (extending for up to approximately 1 μ s in time) for a chemically realistic model of 1,4-polybutadiene (55 % trans, 45 % cis) confined by graphite walls were performed to address the question of the dielectric relaxation behavior of a polymer in confinement. Since polybutadiene is a weakly polar polymer, the partial charges were included after the simulations of the same but nonpolar polymer. Then, using the fluctuation–dissipation theorem which states that the linear response of a given system to an external perturbation is expressed in terms of fluctuation properties of the system in thermal equilibrium, one is able to estimate the dielectric permittivity from the fluctuations of the dipole moments of the

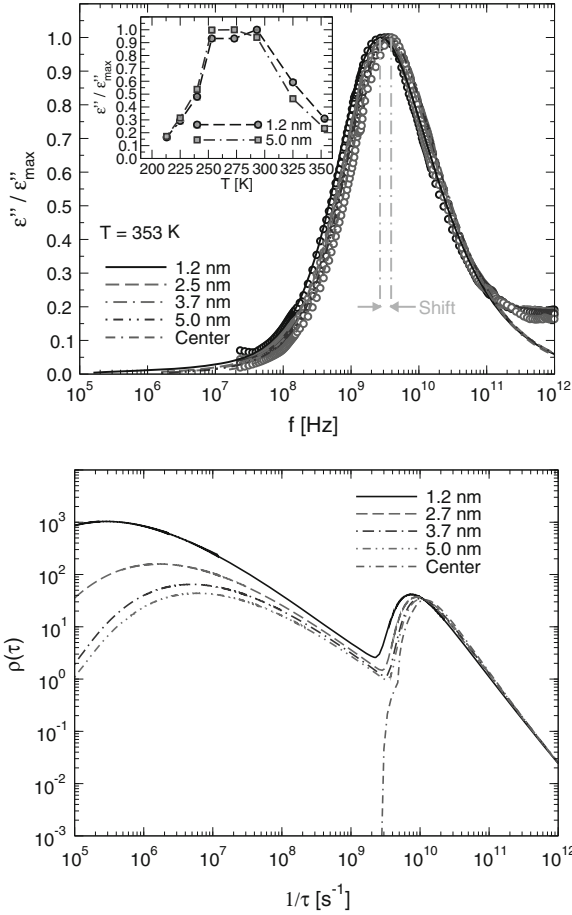


Fig. 8 *Top panel*: frequency dependent dielectric permittivity for $T = 353$ K and several layer thicknesses indicated in the legend. A small shift of the peak position for the thinnest layer of 1.2 nm is indicated. Points are Fourier transforms of the simulation data, lines are transforms of fits, as done in Fig. 4. The inset shows the temperature dependence at two indicated thicknesses at a frequency of $f = 2.25 \cdot 10^8$ Hz. *Bottom panel*: the relaxation time distributions as a function of the inverse of the relaxation time constant at $T = 353$ K. Data are shown for comparable layer thicknesses as in the *top panel*

cis segments in a polymer molecule. The dielectric relaxation functions in the bulk had been studied before for this polymer. The Fourier spectra and the relaxation time distributions were computed from the raw data and from a model fit capturing the data (and also extrapolating the behavior to long times). This allows one to conclude that the confinement introduces mainly a broadening of the frequency spectrum (Fourier space), which, however, is the result of a sum of two unimodal processes according to the relaxation time distributions. We estimated the glass transition for this confined polymer systems using the activation representation, where the frequency of the

maximum dielectric loss is plotted as a function of inverse temperature. When one performs standard VFT fits of the temperature dependence of the maximum loss frequencies, no shift of the extrapolated glass transition temperature with decreasing film thickness is obtained within the error bars.

Since our Molecular Dynamics simulations allow us to study the relaxation behavior spatially well resolved (e.g., focusing on monomers that are no further away from the graphite surface than 1.2 nm), we are able to identify the signals of two distinct slowly relaxing phenomena, both in the time dependence of relaxation functions (see Fig. 4) and in the relaxation time spectrum (see Fig. 8): namely glassy freezing of the same type as in the bulk, and chain desorption kinetics at the graphite wall. The relaxation time distributions of both processes are broad, and due to their somewhat different temperature dependence, they merge in the temperature region of interest. We also show that it is hard to disentangle these processes in the dielectric loss spectra (see Fig. 5).

Acknowledgments The authors are grateful for funding received within the Focused Research Program SPP 1369 of the German Science Foundation. A generous grant of CPU time at the Jülich Supercomputer Center (JUQUEEN and JUROPA) is gratefully acknowledged. We thank F. Kremer and E.U. Mapesa (University of Leipzig, Germany) for stimulating discussions.

References

1. Kremer F, Schönhalz A (2003) Broadband dielectric spectroscopy. Springer, Berlin
2. Bedrov D, Smith GD (2005) Molecular dynamics simulation study of the α - and β -relaxation processes in a realistic model polymer. *Phys Rev E* 71:050801(R)
3. Smith GD, Borodin O, Paul W (2002) A molecular-dynamics simulation study of dielectric relaxation in a 1,4-polybutadiene melt. *J Chem Phys* 117:10350
4. Eslami H, Muller-Plathe F (2009) Structure and mobility of poly(ethylene terephthalate)- a molecular dynamics simulation study. *Macromolecules* 42:8241
5. Bahar I, Erman B, Kremer F, Fischer EF (1992) Segmental motions of cis-polyisoprene in the bulk state: interpretation of dielectric relaxation data. *Macromolecules* 25:816
6. Peter S, Napolitano S, Meyer H, Wübbenhorst M, Baschnagel J (2008) Modeling dielectric relaxation in polymer glass simulations - dynamics in the bulk and in supported polymer films. *Macromolecules* 41:7729
7. Alcoutlabi M, McKenna GB (2005) Effects of confinement on material behaviour at the nanometre size scale. *J Phys Condens Matter* 17:R461
8. Ediger MD (2000) Spatially heterogeneous dynamics in supercooled liquids. *Ann Rev Phys Chem* 51:99
9. Kremer F, Mapesa EU, Tress M (2012) Molecular dynamics of polymers at nanometric length scales: from thin layers to isolated coils. In: Kalmykov YP (ed) Recent advances in broadband dielectric spectroscopy. Springer, Dordrecht
10. Daoulas KC, Harmandaris VA, Mavrantzas VG (2005) Detailed atomistic simulation of a polymer melt / solid interface - structure, density and conformation of a thin polyethylene melt film adsorbed on graphite. *Macromolecules* 38:5780
11. Harmandaris VA, Daoulas KC, Mavrantzas VG (2005) Detailed atomistic simulation of a polymer melt / solid interface - local dynamics and diffusion of a thin polyethylene melt film adsorbed on graphite. *Macromolecules* 38:5796

12. Varnik F, Baschnagel J, Binder K (2002) Reduction of the glass transition temperature in polymer films: a molecular-dynamics study. *Phys Rev E* 65:021507
13. Torres JA, Nealey PF, De Pablo JJ (2000) Molecular simulation of ultrathin polymeric films near the glass transition. *Phys Rev Lett* 85:3221
14. Hudzinsky D, Lyulin AV, Baljon ARC, Balabaev NK, Michels MAJ (2011) Effects of strong confinement on the glass-transition temperature in simulated atactic polystyrene films. *Macromolecules* 44:2299
15. Binder K, Kob W (2011) Glassy materials and disordered solids: an introduction to their statistical mechanics. World Scientific Publishing Company, Singapore
16. Hess B, van der Spoel D, Lindahl E (2008) *J Chem Theory Comput* 4:435. <http://www.gromacs.org>
17. Smith GD, Paul W (1998) United atom force field for molecular dynamics simulations of 1,4-polybutadiene based on quantum chemistry calculations on model molecules. *J Phys Chem A* 102:1200
18. Steele WA (1973) The physical interaction of gases with crystalline solids-i, Gas-solid energies and properties of isolated adsorbed atoms. *Surf Sci* 36:317
19. Zorn R, Mopsik FI, McKenna GB, Willner L, Richter D (1997) Dynamics of polybutadienes with different microstructures - 2. Dielectric response and comparisons with rheological behavior 107:3645
20. Paul W, Smith GD (2004) Structure and dynamics of amorphous polymers - computer simulations compared to experiment and theory. *Rep Prog Phys* 67:1117
21. Smith GD, Borodin O, Bedrov D, Paul W, Qiu X, Ediger MD (2001) ¹³C-NMR spin-lattice relaxation and conformational dynamics in a 1,4-polybutadiene melt. *Macromolecules* 34:5192
22. Smith GD, Paul W, Monkenbusch M, Richter D (2001) On the non-gaussianity of chain motion in unentangled polymer melts. *J Chem Phys* 114:4285
23. Yelash L, Virnau P, Binder K, Paul W (2010) Slow process in confined polymer melts: layer exchange dynamics at a polymer solid interface. *Phys Rev E* 82:050801
24. Yelash L, Virnau P, Binder K, Paul W (2012) Three-step decay of time correlations at polymer-solid interfaces. *Europhys Lett* 98:28006
25. Binder K, Baschnagel J, Paul W (2003) Glass transition of polymer melts: test of theoretical concepts by computer simulation. *Prog Polym Sci* 28:115
26. Stickel F, Fischer EW, Richert R (1995) Dynamics of glass-forming liquids: i - temperature derivative analysis of dielectric relaxation data. *J Chem Phys* 102:6251
27. Stickel F, Fischer EW, Richert R (1996) Dynamics of glass-forming liquids: ii - detailed comparison of dielectric relaxation, dc-conductivity and viscosity data. *J Chem Phys* 104:2043
28. Mapesa EU, Tress M, Schulz G, Huth H, Schick C, Reichle M, Kremer F (2013) Segmental and chain dynamics in nanometric layers of poly(cis-1,4-isoprene) as studied by broadband dielectric spectroscopy and temperature-modulated calorimetry. *Soft Matter*. doi: [10.1039/C3SM51311D](https://doi.org/10.1039/C3SM51311D)
29. Tress M, Mapesa EU, Kossack W, Kipnusu WK, Reiche M, Kremer F (2013) Glassy dynamics in condensed isolated polymer chains. *Science* 341:6152
30. Gradshteyn IS, Ryzhik IM (2007) Table of integrals, series, and products. Academic Press, USA
31. Schwartz L (1966) Mathematics for the Physical Sciences. Herman, Paris

<http://www.springer.com/978-3-319-06099-6>

Dynamics in Geometrical Confinement

Kremer, F. (Ed.)

2014, VIII, 366 p. 184 illus., 116 illus. in color.,

Hardcover

ISBN: 978-3-319-06099-6